Robust subgap edge conduction in bilayer graphene with disordered edge termination

Hyunwoo Lee,[1] Kenji Watanabe,[2] Takashi Taniguchi,[2] Gil-Ho Lee,[1,*] and Hu-Jong Lee[1,†]
[1]*Department of Physics, Pohang University of Science and Technology, Pohang 790-784, Korea*
[2]*National Institute for Material Science, Tsukuba 305-0044, Japan*

(Received 26 February 2020; revised 29 June 2020; accepted 1 July 2020; published 31 July 2020)

The subgap transport in electrostatically gapped bilayer graphene (BLG) is explored by adopting ultrashort constrictions of BLG. We confirmed the emergence of the edge conducting channels, with a residual conductance of $\sim 2e^2/h$ per edge of realistic disorder. Transport along the edge state exhibits either Coulomb blockade oscillations or Fabry-Perot interference, depending on the interfacial transparency between the reservoirs and the edge channel. Both residual conductance and band-gap dependence of the penetration range of the edge state from a constriction edge coincide well with the behavior of the theoretically predicted robust edge conducting channel, which forms irrespective of the degree of edge disorder.

DOI: 10.1103/PhysRevB.102.035448

The nontrivial topological electronic structure [1,2] of gapped bilayer graphene (BLG) [3,4] provides zero-energy states at the boundary between the regions of distinct topological order, which is one of the most distinguishing features from those of ordinary insulators. The electronic transport along the zero-energy states, counterpropagating for two nonequivalent valleys of BLG, is directly linked to the valley-specific pseudospin polarization in the material (see Fig. S1 of the Supplemental Material [5]). Emergence of a topological zero-energy state inside the band gap was proposed [6,7] and observed in BLG at the boundary between regions with either opposite stacking order [8,9] or electrically inverted band gaps [10,11]. The counterpropagating valley-chiral mode for different valleys inside the band gap was predicted to emerge at ideally zigzag-terminated edges of BLG [12,13], with conductance of $2e^2/h$ per edge with spin degeneracy [14] (e: electron charge; h: Planck's constant).

However, observation of this topologically nontrivial edge state has proven elusive due to unavoidable atomic disorder at the physically tailored graphene edges, which causes severe intervalley scattering. Nevertheless, it has been theoretically predicted that a conducting edge state can exist in a spatially localized form even in the presence of strong atomic disorder at graphene edges, either structural or chemical [1]. According to the theory, the edge state at a randomly distributed zigzag segment is predicted to decay exponentially into the bulk from the edge with a penetration range (d), which is closely associated with the band gap (E_{gap}) of BLG. The penetrated edge states overlap with each other, forming a conducting channel along an edge with a localization length (λ) of tens of nanometers, which is proportional to d [1]. For a d much larger than the interatomic distance of BLG ($a \sim 0.14$ nm), the electronic transport along the edge channel within the localization length is less affected by the atomic disorder confined to an edge, leading to the mean free path comparable to λ [1]. This forms a robust edge conducting channel with valley-selective chirality, irrespective of the degree of edge disorder, as long as the length of device is within λ. Although the one-dimensional (1D) edge transport has been suggested by recent studies on gapped BLG via scaling analysis [15] and superconducting interferometry [16,17], the evidence for the topological nature of the 1D edge transport has not been explicitly confirmed to date. In this study, we illustrate experimentally that the edge conducting channels emerge in gapped BLG constrictions, where observed ballistic edge conductance and E_{gap} dependence of d indicate that the corresponding edge conducting state is topologically nontrivial.

Devices in this study consist of a dual-gated nanoconstriction that is connected to bottom-only-gated BLG reservoirs, as shown in the schematics in Figs. 1(a) and 1(b). For the fabrication, we first prepared a heterostructure incorporating graphite (Gr), hexagonal boron nitride (hBN), and BLG (Gr/hBN/BLG/hBN/Gr), by multiple dry transfer processes [18], where the top and bottom Gr layers were employed for dual gating. A metallic mask of a Cr/Au (3/12 nm) bilayer stack for the top-gate lead was deposited on top of the Gr/hBN/BLG/hBN/Gr heterostructure. The part of the top Gr layer that was not covered with the metallic mask was removed by reactive ion etching, to separate the dual-gated constriction from the BLG reservoirs. An ultrashort constriction was realized by the undercut etching technique [19] with the use of a 30-nm-thick Al_2O_3 mask layer [not shown in Fig. 1(a) for simplicity]. More details of fabrication processes are described in the Supplemental Material [5]. In the main text, we focus on the results from a representative device A, among eight devices with different lengths L and widths W (see Table S1 of the Supplemental Material [5]). The physical dimensions of the constrictions (i.e., $L \sim 50$ nm and $W \sim 650$ nm for device A) were determined by scanning electron microscopy (SEM). Except for the temperature dependence measurements, all of the transport data were obtained at 4.2 K.

Figure 1(c) shows a color-coded plot of the zero-bias constriction resistance (R) obtained under configuration 1 given

*Corresponding author: lghman@postech.ac.kr
†Corresponding author: hjlee@postech.ac.kr

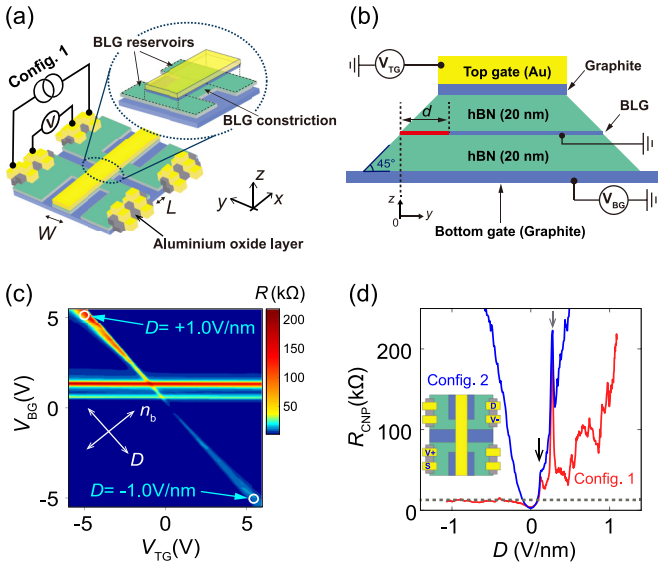

FIG. 1. (a) Schematic of the BLG constriction with a four-probe measurement configuration (configuration 1); the serial resistance of the BLG reservoirs was only a few hundreds of ohms. (b) Schematic of a cross-sectional view of the BLG constriction with the penetration range (d) of conducting state (red) from an edge. (c) Color-coded plot of the four-probe zero-bias resistance of the BLG constriction, measured at 4.2 K as a function of the top gate voltage (V_{TG}) and bottom gate voltage (V_{BG}). (d) Resistance at the charge neutrality point (CNP, R_{CNP}) is plotted as a function of the displacement field (D) for two different measurement configurations. The red and blue curves correspond to configuration 1 of (a) and configuration 2 of the inset in (d), respectively. The grey dotted line represents the resistance value of $h/2e^2$. Resistance peaks in both curves (grey and black arrows) correspond to the CNP of each of the bottom-only-gated BLG reservoirs.

in Fig. 1(a), as a function of the top gate voltage (V_{TG}) and bottom gate voltage (V_{BG}) using the low-frequency (7.78 Hz) lock-in technique (all results were obtained under configuration 1, unless stated otherwise). Using a parallel-plate capacitor model, the bulk carrier density (n_b) and displacement field (D) for the bulk of the constriction are expressed by $n_b = C^A_{TG}(V_{TG} - V^0_{TG})/e + C^A_{BG}(V_{BG} - V^0_{BG})/e$ and $D = C^A_{BG}(V_{BG} - V^0_{BG})/2\varepsilon_0 - C^A_{TG}(V_{TG} - V^0_{TG})/2\varepsilon_0$, where $C^A_{BG(TG)}$ is the bottom (top) gate capacitance per unit area and $V^0_{BG(TG)}$ is the bottom (top) gate voltage of the charge neutrality point (CNP). The top and bottom hBN layers have the same thickness (t_{hBN}) of 20 nm, thus we have the capacitance ratio $C^A_{TG}/C^A_{BG} \sim 1$, which corresponds to the absolute slope of the CNP line in Fig. 1(c). The two horizontal enhanced-resistance lines in Fig. 1(c) correspond to the CNPs of the two bottom-only-gated reservoirs, which are not coincident because of possible unintended doping of the top layer of BLG during device fabrication.

To see the details of the emerging signature of the edge state involved in the transport, the resistance at the CNP (R_{CNP}) measured in two different configurations is plotted as a function of D in Fig. 1(d). When measured across the dual-gated BLG in configuration 2 [inset of Fig. 1(d)], the edge channels are not connected between the bottom-only-gated BLG reservoirs in the sides of the source and drain. Thus R_{CNP} in this case represents the conduction through the bulk of the BLG, and increases as the bulk band gap grows with increasing magnitude of D (see Fig. S6 in the Supplemental Material for more data [5]). Meanwhile, for configuration 1, R_{CNP} represents the conduction mainly along an edge channel on one side of the nanoconstriction, and is therefore saturated as D becomes more negative. In configuration 1 with large $|D|$, the bulk BLG is insulating so that the edge state at one side of the constriction provides the only conducting channel for residual conductance of $2e^2/h$ [grey dotted line in Fig. 1(d)]. The saturation behavior of the conduction close to $2e^2/h$ provides clear evidence for ballistic and valley-specific chiral transport in the topological edge states in the ultrashort constriction. On the other hand, measurements obtained on relatively long constrictions of $L > 200$ nm showed significantly suppressed residual conductance (see Fig. S4), which suggests that the edge states are localized with a characteristic length λ that is significantly shorter than $\sim$200 nm [1].

We attribute the asymmetric R_{CNP} vs D in configuration 1 to different D-dependent coupling between a BLG reservoir and the edge state of the BLG constriction at the interface. Maintaining the dual-gated bulk region of the BLG constriction at the CNP, BLG reservoirs are either electron (n)-doped for positive D or hole (p)-doped for negative D, as they are only affected by the bottom gate. The D dependence of R_{CNP} for configuration 1 suggests that the *edges of the nanoconstriction* were heavily p-doped irrespective of gate voltages. Then, a p-n' barrier would have formed [20] at the interface between the n-doped reservoir and the p-doped edge-localized state for positive D [Fig. 2(a)]. This led to lower transmission than that of a unipolar p-p' barrier for negative D. We argue that such heavy p doping at the edges was due to the exposure of the edges to oxygen plasma during the etching process [21]. In fact, we observed that the asymmetry in R_{CNP} was inverted when recooling the same device after exposing it to air at room temperature [Fig. S5(b) of the Supplemental Material [5]]. Interestingly, the original asymmetry of R_{CNP} of the air-exposed device was resumed when the device was reexposed to oxygen plasma [Fig. S5(c) [5]]. This suggests that the doping of edges is mainly determined by the ambient conditions to which the edges are exposed.

Here we discuss the gate- and bias-voltage dependence of the edge-state transport in the context of the low transmission for positive D. Figure 2(b) shows the zero-bias conductance (G) in configuration 1 as a function of n_b at fixed $D = 1.0$ V/nm [see Fig. 1(c)]. In a highly hole-doped regime ($n_b < 0$), a p-n' barrier forms between the *bulk of the BLG constriction* and the BLG reservoirs so that the conductance is smaller than that in the highly electron-doped regime ($n_b > 0$). Near the CNP, where the bulk of the BLG constriction is insulating, the conductance is much smaller than $2e^2/h$ and shows Coulomb blockade (CB) oscillations [inset of Fig. 2(b)]. In the shaded region of Fig. 2(b), Coulomb diamonds are also revealed in the source-drain bias (V_{SD}) dependence of the differential conductance dI/dV [Fig. 2(c)]. Observation of the CB behavior suggests that the edge state forms a quantum dot (QD) connected to the BLG reservoirs with low transmission [22]. As no magnetic impurities are expected in the constriction, the alternating intervals of n_b

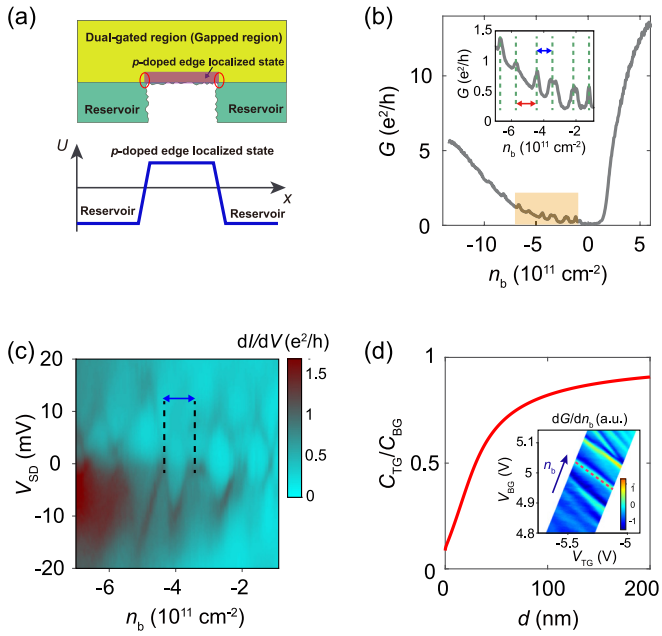

FIG. 2. (a) Upper panel: schematic top view of one of the edges. The purple region represents the edge conducting channel located at one side of the constriction. Red circles denote the location of partially opaque p-n interfaces between the edge state and the reservoirs. Lower panel: schematic configuration of the electrochemical potential (U) of the electron-doped reservoirs and hole-doped edge state. (b) Zero-bias differential conductance (G) plotted as a function of n_b with a fixed displacement field $D = +1.0\,\mathrm{V/nm}$. Near the CNP (shaded area), Coulomb blockade oscillations are observed. Inset: a magnified plot of the shaded region. The alternating intervals of n_b between the resonant conductance peaks (red and blue arrows) indicate two-fold shell filling in the QD. (c) Color-coded differential conductance dI/dV versus source-drain bias (V_{SD}) and n_b. (d) Gate capacitance ratio C_{TG}/C_{BG} as a function of d into the bulk BLG. This was estimated by numerical calculation based on the configuration shown in Fig. 1(b) (see Fig. S14 for details [5]). Inset: transconductance dG/dn_b as a function of V_{TG} and V_{BG} for $D \sim 1.0\,\mathrm{V/nm}$.

between resonant conductance peaks [red and blue arrows in the inset of Fig. 2(b)] indicates that the edge state has only spin degeneracy [23], which corresponds to the valley-specific chiral transport along the topological edge states. The Coulomb diamonds of comparable heights to each other in V_{SD} without overlap suggests the presence of a single QD along the edge of the constriction [24]. The smaller spacing in n_b between oscillations [blue arrows in the inset of Figs. 2(b) and 2(c)] is related to the charging energy of the QD. The Coulomb diamonds are better developed for large values of D and disappear for $D < 0.6\,\mathrm{V/nm}$, where the p-n' barrier between the QD at the edge and the BLG reservoirs becomes weaker, along with gradual delocalization of the QD (see Sec. S6 of the Supplemental Material [5] for more data).

For quantitative analysis of the top and bottom gate efficiency for the QD at the edge, we measured transconductance (dG/dn_b) with respect to V_{BG} and V_{TG} for $D \sim 1.0\,\mathrm{V/nm}$, as shown in inset of Fig. 2(d). From the slope of the resonant peak (red dotted line in the inset), we obtained the capacitance ratio of the top to bottom gate for the QD, $C_{TG,\,QD}/C_{BG,\,QD} = 0.36$, which is in sharp contrast to the bulk value of $C^A_{TG}/C^A_{BG} = 1$. This discrepancy may be understood by the stray electric field at the QD located at the edge [25]. A numerical simulation on the effect of a stray electric field (see Fig. S14 [5]) can be used to estimate the capacitance ratio (C_{TG}/C_{BG}) for the edge state with different penetration ranges [d, see Fig. 2(d)]. Here, for simplicity, we assume a rectangular shape of QD with length (L_{QD}) along the length of the BLG constriction and depth ($d_{QD} = d$) into the bulk BLG, with an inclined angle of $\sim 45^\circ$ at the edge of the hBN/BLG/hBN stack [18,19]. Combining the observed value of $C_{TG,\,QD}/C_{BG,\,QD} = 0.36$ and the electric-field simulation in Fig. 2(d) yields $d_{QD} = 19\,\mathrm{nm}$. Then, the capacitance per unit area for the QD is obtained as $C^A_{TG,QD} = 0.50\ C^A_{bulk}$ for the top gate and $C^A_{BG,QD} = 1.4\ C^A_{bulk}$ for the bottom gate, where $C^A_{bulk} = C^A_{TG} = C^A_{BG} = \varepsilon_{hBN}\varepsilon_0/t_{hBN}$ with a relative dielectric constant of hBN ($\varepsilon_{hBN} = 3.9$) and vacuum permittivity (ε_0). The difference between $C^A_{TG,QD}$ and $C^A_{BG,QD}$ mainly arises from the difference in coverage between the top and bottom gate electrode on the QD. The gate capacitance for the QD is also estimated from the size of the diamonds, $\Delta n_b \sim 1.0 \times 10^{11}\,\mathrm{cm^{-2}}$ [blue arrows in the insets of Figs. 2(b) and 2(c)], which corresponds to a change of V_{TG} ($\Delta V_{TG,QD} = 0.05$ V) and V_{BG} ($\Delta V_{BG,QD} = 0.05\,\mathrm{V}$). Using the relationship $e = C_{TG,\,QD}\Delta V_{TG,QD} + C_{BG,\,QD}\Delta V_{BG,QD}$ and $C_{TG,\,QD}/C_{BG,\,QD} = 0.36$, we obtain $C_{TG,QD} = 0.87$ aF and $C_{BG,QD} = 2.4$ aF. Combining these with the areal capacitance, the area of QD is estimated to be $A = L_{QD}d_{QD} = C_{BG,QD}/C^A_{BG,QD} = 1010\,\mathrm{nm^2}$. With $d_{QD} = 19\,\mathrm{nm}$, we obtain $L_{QD} = 52\,\mathrm{nm}$, which corresponds to λ. The dimensions of edge localized states estimated from this analysis, combining Coulomb blockade feature and electrostatic field simulation, match well with the physical length of the constriction, $L \sim 50\,\mathrm{nm}$, determined by SEM. This suggests that our simplified model of the edge state is reliable. The discrepancy in the value of λ between the numerical simulation ($\sim$20 nm) [1] and the estimation in our device ($\sim$50 nm) may be caused by the detailed disorder profile in the edge of a real device. Here, it should be emphasized that d is a more fundamental physical quantity of edge state, which is to be compared with the theoretical prediction, rather than λ. d can be estimated by determining the band gap of BLG, but λ may vary with the details of the edge structure. In the simulation [1] the localization length is predicted to be $\lambda \sim cd$ with a constant c ($\sim$5) for particular realization of edge disorder.

Now we focus on the edge-state transport for high transmission at negative D. Figure 3(a) shows the conductance G for configurations 1 and 2 with respect to n_b at a fixed value of $D = -1.0\,\mathrm{V/nm}$ [see Fig. 1(c)]. The subgap conductance in configuration 1 is predominantly from an edge conducting channel, as the insulating bulk of BLG provides the subgap conductance lower than $\sim 0.1e^2/h$ as estimated from G in configuration 2 [blue curve in Fig. 3(a)]. In contrast to the QD behavior for low transmission, the conductance of the edge conducting channel near the CNP is close to $\sim 2e^2/h$, which corresponds to the ballistic-limit value of the subgap edge state with valley polarization. Furthermore, we observed conductance oscillations [green arrows in Fig. 3(a)] in configuration 1, which become prominent in the gapped region

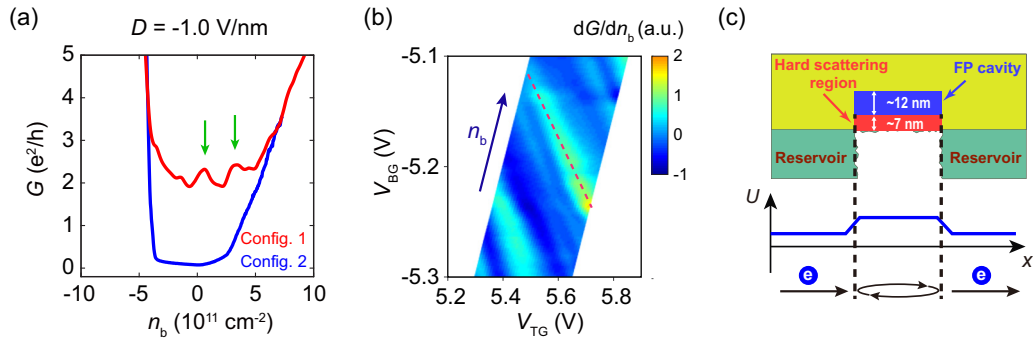

FIG. 3. (a) Zero-bias differential conductance (G) vs the carrier density of bulk n_b in measurement configurations 1 (red) and 2 (blue), with a fixed displacement field $D = -1.0$ V/nm. G in configuration 1 shows resonant peaks (green arrows) near the CNP. (b) Dual-gated transconductance dG/dn_b is plotted as a function of V_{TG} and V_{BG} near $D = -1.0$ V/nm. (c) Upper panel: schematic top view of the expected conducting channel through the edge state at $|D| = 1$ V/nm. The outermost red rectangle close to the disordered edge and the inner blue rectangle represent the hard scattering region and the ballistically conducting channel (FP cavity), respectively. Middle panel: a schematic configuration of the electrochemical potential (U) of the hole-doped reservoirs and hole-doped edge state. Lower panel: a schematic illustrating the FP interference path in the edge channel (blue region).

near the CNP. However, the oscillations almost vanish with increasing temperature while the background conductance increases (see Fig. S11 [5]), which arises as the transport only along the edge of the constriction at low temperatures diffuses into the entire constriction including the bulk at high temperatures. Variations of the differential conductance ($\Delta dI/dV$) as a function of V_{SD} and n_b for negative values of D by subtracting the smooth background from dI/dV produces a checkerboard feature (Fig. S9 [5]). These indicate that the subgap transport exhibits Fabry-Perot (FP) interference, arising as electrons are partially reflected at the interfaces between the edge channel and the BLG reservoirs. Whenever the traveling electrons in the edge channel accumulate the dynamic phase of modulo 2π, the constructive interference induces resonant conductance peaks. Both subgap conductance and the signature of FP interference provide strong evidence for ballistic transport of the edge state within the length of the constriction [26,27].

The observation of ballistic transport of the subgap edge state may seem surprising since the edge of BLG constrictions was physically tailored using oxygen plasma, with substantial random edge disorder, either structural or chemical. We estimated the size of d of the edge states to be $\sim$19 nm for $|D| = 1$ V/nm, which is extracted from the Coulomb blockade features at $D = 1.0$ V/nm, considering the fact that the value of d of the edge state should depend only on the magnitude of D but not on its polarity. The penetration range in our measurements is predicted to be tens of nanometers, which is much larger than the interatomic distance of BLG ($a \sim 0.14$ nm). As a result, the edge states penetrated into the bulk could be far less affected by atomic disorders confined to the edges, leading to the formation of a ballistic 1D conducting channel inside the bulk [blue rectangle in Fig. 3(c)]. The dual-gated transconductance map near $D \sim -1.0$ V/nm is shown in Fig. 3(b). From the slope of the resonant peak, we obtain the capacitance ratio of the FP cavity for the top and bottom gates, $C_{TG,FP}/C_{BG,FP} \sim 0.53$. For the same magnitude of D, the observed value of capacitance ratio for the FP interference turns out to be larger than the one for the CB oscillations ($C_{TG,FP}/C_{BG,FP} > C_{TG,\,QD}/C_{BG,\,QD} (\sim 0.36)$, at $|D| = 1$ V/nm). This supports that part of the edge-localized state away from the edge, where most of the short-ranged scatterers reside, forms a ballistic edge conducting channel [blue rectangle in Fig. 3(c)], because the capacitance ratio for the blue rectangle ($C_{TG,FP}/C_{BG,FP}$) is larger than the one for the entire region of the edge state ($C_{TG,\,QD}/C_{BG,\,QD}$) corresponding to the red and blue rectangular regions combined. Comparing with the simulation result, the observed $C_{TG,FP}/C_{BG,FP} \sim 0.53$ corresponds to a 12-nm-wide FP cavity that is located in the range of 7–19 nm inward from an edge (see Sec. S10 of the Supplemental Material for details [5]). We thus roughly consider that the 7-nm-wide outermost part of the edge channel [red rectangle in Fig. 3(c)] was not involved in the ballistic transport due to severe short-range scattering there. The capacitance of each gate per unit area for the FP cavity, the blue-rectangular region in Fig. 3(c), is estimated to be $C^A_{TG,FP} = 0.59C^A_{bulk}$ for the top gate and $C^A_{BG,FP} = 1.1C^A_{bulk}$ for the bottom gate. FP conductance peaks occur under the constructive interference condition $\Delta k_F = \pi/L_{FP}$, where Δk_F is the difference of Fermi wave number between successive conductance peaks and L_{FP} is the FP cavity length. Considering the edge state as a 1D system without valley degeneracy, the carrier density of FP cavity per unit length is expressed as $n^L_{FP} = 2k_F/\pi$. Then the interval between adjacent FP conductance peaks $\Delta n^L_{FP} = 2\Delta k_F/\pi$ corresponds to a change in V_{TG} of $\Delta V_{TG,FP} = 0.13$ V, and in V_{BG} of $\Delta V_{BG,FP} = 0.13$ V [green arrows in Fig. 3(a)], i.e., $\Delta n^L_{FP} = (C^L_{TG,FP}\Delta V_{TG,FP} + C^L_{BG,FP}\Delta V_{BG,FP})/e$, where $C^L_{TG(BG),FP} = d_{FP}C^A_{TG(BG),FP}$ is the capacitance per unit length of the FP cavity for the top (bottom) gate. Thus, the length of the FP cavity is estimated to be $L_{FP} = 2/\Delta n^L_{FP} \sim 70$ nm for $D = -1$ V/nm, which is somewhat longer than the actual length of the constriction, $L \sim 50$ nm.

Topologically trivial edge states can also be generated by local doping of BLG in a stray electric field from the top and bottom gates. According to the numerical simulation in Fig. 4(a), as $|D|$ increases, the trivial edge states accumulate more carriers while expanding deeper into the bulk BLG. Thus, the stray field applied to the edge will lead to an increase in residual conductance at the CNP with increasing $|D|$, which

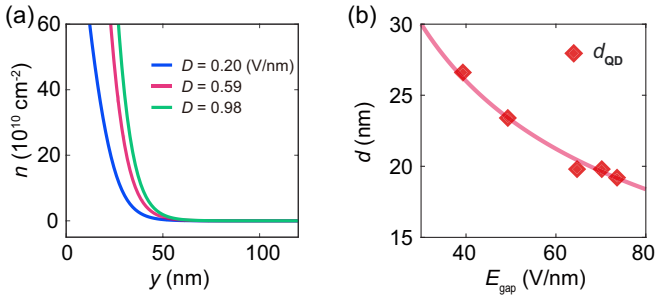

FIG. 4. (a) Numerical calculation of the carrier-density accumulation as a function of the distance (y) from the edge at different D. (b) The penetration range d estimated from the QD behaviors is plotted with respect to E_{gap}. The red line represents the best fit to the theoretical prediction for the penetration range ($d = \alpha\hbar/\sqrt{mE_{\mathrm{gap}}}$) for $\alpha \sim 3.3$.

is contrary to the saturation of conductance shown in Fig. 1(d) for high values of negative $|D|$. Meanwhile, the previous study using the superconducting interferometry showed that edge conduction in gapped BLG occurs regardless of the existence of additional charge accumulation at the edges [16]. This result supports that the edge conduction observed in our study can occur even in the absence of additional charge accumulation by either stray field or chemical doping.

The penetration range of edge states in the limit of strong disorder was predicted to be an order $\sim\hbar/\sqrt{mE_{\mathrm{gap}}}$ [28], where m is the effective mass of electron in BLG and $\hbar$ is the reduced Planck constant [1]. We fit d estimated from the QD behavior to $d = \alpha\hbar/\sqrt{mE_{\mathrm{gap}}}$ [red line in Fig. 4(b)] with α as a constant of order unity. Both the order of magnitude and the E_{gap} dependence of d well match the theoretical prediction, which provides additional strong evidence that the edge conduction in our gapped BLG originated from the topologically nontrivial edge states.

At low temperatures, the residual conductance in gapped BLG is predicted to be governed by the localization length of edge states as far as impurity-mediated conducting channels in the bulk of BLG are suppressed [29]. According to the theoretical calculation [1], the edge localization length is proportional to the d, regardless of the strength of edge disorder. Four different BLG constrictions used in this study, with comparable length of ~50 nm, showed that the residual conductance with negative D side is either $\sim 2e^2/h$ (devices A and B) or $\sim 4e^2/h$ (devices C and D), depending on the number of edges involved in the transport (see Fig. S3 and Table S1 [5]). This reconfirms that the length of the constrictions ($L \sim 50$ nm) is smaller than the localization length, and that the residual conductance in gapped BLG arises from the subgap edge states with valley-associated chirality.

In sum, we report detailed subgap conductance measurements in BLG constrictions. The observed Coulomb blockade oscillations and Fabry-Perot interference in the ultrashort devices indicate the formation of quantum dot structure and ballistic transport, respectively, with the residual conductance close to $\sim 2e^2/h$ per edge. Together with an analysis, this strongly indicates that it was hosted by the ballistic and robust valley-specific edge conducting channels, irrespective of the degree of edge disorder, as long as the length of device is within the localization length, confirming the theoretical prediction [1]. It may seem to be counterintuitive to have ballistic transport along a randomly disordered edge of BLG. However, penetration of the edge states into the bulk of gapped BLG with a range much larger than the in-plane interatomic distance drives carriers to detour atomic disorders at the edges, leading to the formation of 1D conducting channel away from the edge. In this case, carriers within the localization length experience much weaker potential of the edge disorder, thus avoiding scattering and intervalley mixing. Both the near convergence of the conductance per channel and the band gap dependence of the penetration range of the edge state from a constriction edge, observed in this study, indicate robustness of the edge state, which is rooted in the underlying topology of the bulk band structure of BLG, even in the absence of the strong topological protection of time-reversal symmetry. The insensitivity of the edge state to the edge disorder and its robustness in gapped BLG provide a pivotal step forward for the fault-tolerant and *in situ* controllable device realization based on topological states.

This work was supported by the National Research Foundation (NRF) through the SRC Center for Topological Matter, POSTECH, Korea (Grant No. 2018R1A5A6075964 for H.-J.L.), Samsung Science and Technology Foundation, Korea (Project No. SSTF-BA1702-05 for G.-H.L.), and the Elemental Strategy Initiative conducted by the MEXT, Japan (Grant No. JPMXP0112101001), JSPS KAKENHI, Japan (Grant No. JP20H00354), and the CREST of JST, Japan (JPMJCR15F3) for K.W. and T.T.

[1] J. Li, I. Martin, M. Buttiker, and A. F. Morpurgo, Nat. Phys. **7**, 38 (2011).

[2] J. Li, A. F. Morpurgo, M. Büttiker, and I. Martin, Phys. Rev. B **82**, 245404 (2010).

[3] Y. Zhang, T.-T. Tang, C. Girit, Z. Hao, M. C. Martin, A. Zettl, M. F. Crommie, Y. R. Shen, and F. Wang, Nature (London) **459**, 820 (2009).

[4] M. Edward and K. Mikito, Rep. Prog. Phys. **76**, 056503 (2013).

[5] See Supplemental Material at http://link.aps.org/supplemental/10.1103/PhysRevB.102.035448 for details on schematics of the band structure of gapped BLG with ideal zigzag edge termination, device fabrication, resistance saturation in R_{CNP} for different devices, dual-gated resistance maps for thermal recycling, dual-gated resistance maps for configurations 1 and 2, Coulomb blockade patterns of edge-localized states in the QD regime, phase-coherent transport across the edge-localized states in the FP regime, temperature dependence of electrical transport for opposite polarities of D, numerical simulation on the effect of a stray field, and estimation of the location of the FP cavity for $|D| = 1$ V/nm.

[6] I. Martin, Y. M. Blanter, and A. F. Morpurgo, Phys. Rev. Lett. **100**, 036804 (2008).

[7] A. Vaezi, Y. Liang, D. H. Ngai, L. Yang, and E.-A. Kim, Phys. Rev. X **3**, 021018 (2013).

[8] L. Ju, Z. Shi, N. Nair, Y. Lv, C. Jin, J. Velasco Jr., C. Ojeda-Aristizabal, H. A. Bechtel, M. C. Martin, A. Zettl, J. Analytis, and F. Wang, Nature (London) **520**, 650 (2015).

[9] L.-J. Yin, H. Jiang, J.-B. Qiao, and L. He, Nat Commun. **7**, 11760 (2016).

[10] J. Lee, K. Watanabe, T. Taniguchi, and H.-J. Lee, Sci. Rep. **7**, 6466 (2017).

[11] J. Li, K. Wang, K. J. McFaul, Z. Zern, Y. Ren, K. Watanabe, T. Taniguchi, Z. Qiao, and J. Zhu, Nat. Nanotechnol. **11**, 1060 (2016).

[12] E. V. Castro, N. M. R. Peres, J. M. B. Lopes dos Santos, A. H. Castro Neto, and F. Guinea, Phys. Rev. Lett. **100**, 026802 (2008).

[13] W. Yao, S. A. Yang, and Q. Niu, Phys. Rev. Lett. **102**, 096801 (2009).

[14] J. Jung, F. Zhang, Z. Qiao, and A. H. MacDonald, Phys. Rev. B **84**, 075418 (2011).

[15] Md. A. Aamir, P. Karnatak, A. Jayaraman, T. P. Sai, T. V. Ramakrishnan, R. Sensarma, and A. Ghosh, Phys. Rev. Lett. **121**, 136806 (2018).

[16] M. J. Zhu, A. V. Kretinin, M. D. Thompson, D. A. Bandurin, S. Hu, G. L. Yu, J. Birkbeck, A. Mishchenko, I. J. Vera-Marun, K. Watanabe, T. Taniguchi, M. Polini, J. R. Prance, K. S. Novoselov, A. K. Geim, and M. Ben Shalom, Nat. Commun. **8**, 14552 (2017).

[17] M. T. Allen, O. Shtanko, I. C. Fulga, A. R. Akhmerov, K. Watanabe, T. Taniguchi, P. Jarillo-Herrero, L. S. Levitov, and A. Yacoby, Nat. Phys. **12**, 128 (2015).

[18] L. Wang, I. Meric, P. Y. Huang, Q. Gao, Y. Gao, H. Tran, T. Taniguchi, K. Watanabe, L. M. Campos, D. A. Muller, J. Guo, P. Kim, J. Hone, K. L. Shepard, and C. R. Dean, Science **342**, 614 (2013).

[19] H. Lee, G.-H. Park, J. Park, G.-H. Lee, K. Watanabe, T. Taniguchi, and H.-J. Lee, Nano Lett. **18**, 5961 (2018).

[20] B. Huard, J. A. Sulpizio, N. Stander, K. Todd, B. Yang, and D. Goldhaber-Gordon, Phys. Rev. Lett. **98**, 236803 (2007).

[21] I. Childres, L. A. Jauregui, J. Tian, and Y. P. Chen, New J. Phys. **13**, 025008 (2011).

[22] K. Grove-Rasmussen, H. I. Jørgensen, and P. E. Lindelof, Physica E (Amsterdam, Neth.) **40**, 92 (2007).

[23] X. Wang, Y. Ouyang, L. Jiao, H. Wang, L. Xie, J. Wu, J. Guo, and H. Dai, Nat. Nanotechnol. **6**, 563 (2011).

[24] K. Todd, H.-T. Chou, S. Amasha, and D. Goldhaber-Gordon, Nano Lett. **9**, 416 (2009).

[25] P. G. Silvestrov and K. B. Efetov, Phys. Rev. B **77**, 155436 (2008).

[26] P. Rickhaus, R. Maurand, M.-H. Liu, M. Weiss, K. Richter, and C. Schönenberger, Nat. Commun. **4**, 2342 (2013).

[27] A. V. Kretinin, R. Popovitz-Biro, D. Mahalu, and H. Shtrikman, Nano Lett. **10**, 3439 (2010).

[28] The penetration range of the edge states in the presence of realistic edge disorder is predicted to be $d \sim l_0/\sqrt{\Delta}$, where $l_0 = 3ta/2t_\perp$, $\Delta = E_{\rm gap}/2t_\perp$, t and $t_\perp$ describe the intralayer and interlayer hopping energy, respectively [1]. The electron mass in BLG can be expressed as $m = 4\hbar^2 t_\perp/3a^2t^2$, which leads to $d \sim \sqrt{6}\hbar/\sqrt{mE_{\rm gap}}$.

[29] H. Miyazaki, K. Tsukagoshi, A. Kanda, M. Otani, and S. Okada, Nano Lett. **10**, 3888 (2010).